ELSEVIER

Journal of Photochemistry and Photobiology A: Chemistry 143 (2001) 119–127

Journal of Photochemistry and Photobiology A:Chemistry

www.elsevier.com/locate/jphotochem

Photophysical properties of 2,5-diphenyl-thiazolo[5,4-*d*]thiazole

M.R. Pinto, Y. Takahata, T.D.Z. Atvars*

Instituto de Química, Caixa Postal 6154, Unicamp, Campinas, CEP 13083-970, SP, Brazil

Received 27 February 2001; received in revised form 29 June 2001; accepted 3 July 2001

Abstract

2,5-Diphenyl-thiazolo[5,4-*d*]thiazole (DTTz) was prepared and its photophysical properties were determined by optical absorption and steady-state spectroscopy, both in solution and in the solid state. Solvents with different properties (polarity, dielectric constant and refractive index) were employed and the solvatochromic effect and Stokes's shift were analyzed by Lippert's equation. The fluorescence emission was a mirror image of the excitation (absorption) spectrum, indicating that no geometric distortion takes place upon excitation. Larger Stokes's shifts with significant broadening of the fluorescence emission were obtained in the presence of strong concentrated acidic solutions. There was also a simultaneous decrease of the fluorescence quantum yield. Quantum mechanical calculation shows that this molecule is planar in the electronic ground state and its dipole moment is null in this state. Quantum mechanics successfully simulates the spectral profile. The lower electronic transition is characterized as a π–π^*. Charge densities determined by quantum mechanical calculation demonstrate that protonation occurs on the nitrogen atom of the heterocyclic ring. Although no excimer emission was detected in concentrated solutions and in the solid state, an exciton splitting of the absorption or excitation spectra was observed. This was explained on the basis of the excitonic spectral splitting by the π-stage molecular configuration of the molecules in the solid state with parallel dipole moments.

Keywords: 2,5-Diphenyl-thiazolo[5,4-*d*]thiazole; Fluorescence; Electronic absorption; Heterocyclic chromophore; Spectral simulation

1. Introduction

Conjugated molecules and polymers bearing heterocyclic units are potentially important as optically electroactive materials. Two classes of these optically active materials have recently been studied: photoluminescent heterocyclic compounds, such as benzoquinolines, benzoxazoles, 2,5-diphenylfuran, 1,2-diphenylindole, oxadiazoles, and phthalocyanines, which exhibit high photoluminescence efficiency in solution [1,2]; and, photoconductive and electroluminescent compounds for electroluminescent devices (LED), some of which consist of heterocyclic compounds [3].

The requirement for an electroactive material is the electron donor or acceptor capability to participate in electron conjugation. The presence of a heteroatom in the molecule induces either electron or hole injection/transportation and the molecule may potentially behave as a material displaying charge transport or blocking electroactive layers [4–6]. Thiophene and pyrrole based molecules are examples of "electron-excessive" aromatic rings exhibiting these properties. These compounds are susceptible to chemical and electrochemical oxidation behaving as a p-dopable center. In contrast, the n-dopable heterocycle compounds, such as pyridine and quinoline based chromophores, contain an electron-withdrawing group susceptible to reduction. Likewise, they are known as "electron-accepting" aromatic rings. Examples of n-dopable materials are conjugated molecules and polymers containing non-fused bithiazole units [7] that also present interesting electrochemical/electrochromic [8] and electroluminescent properties [9,10]. The presence of non-bonding electrons on the heteroatom of the thiazole π-conjugated system provides the intrinsic basic center responsible for these properties. The potential application of these compounds as fluorescent probes and sensors is related to their ability to coordinate with transition metal ions [11].

Five-member heterocyclic rings based chromophores also overwhelms electrochemical and photochemical behavior. When the molecule contains two adjacent ring units a higher coplanarity is achieved, absent in oligophenylenes type molecules, resulting in a larger conjugation length that improves somewhat the optical and electric properties [12,13].

Among other five-member ring heterocyclic structures, thiazole is an important π-conjugated building block. Several commercial fluorescent dyes and brighteners bearing the thiazole unit have been produced worldwide. The high hyperpolarizability of some molecules with heterocycle

* Corresponding author. Tel.: +55-1937883078.
E-mail address: tatvars@iqm.unicamp.br (T.D.Z. Atvars).

1010-6030/01/$ – see front matter
PII: S1010-6030(01)00520-2

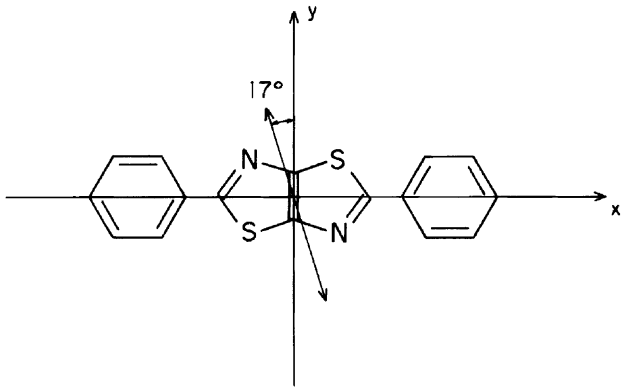

Scheme 1. Molecular structure of the DTTz.

structure is due to the possible bridge formation between the electron-donor and electron-withdrawing conjugated sequences, as was observed in molecules containing benzobisthiazole units [14]. Fiber and liquid crystalline polymers bearing benzobithiazole units exhibit high ultraviolet light and thermal stability [15,16].

2,5-Diphenyl-thiazolo[5,4-*d*]thiazole (DTTz) (Scheme 1) is a compound that contains a bicyclic central unit formed by two thiazole-fused rings. The fused rings confer rigidity and higher planarity to the molecule and improve the conjugative electron transport. Synthesis of this compound can be performed by condensation of aromatic aldehydes with dithiooxamide [17–20]. Studies of the structure [21], spectroscopic properties [22–24], liquid crystallinity [25,26], and conductivity properties of doped compounds [27] and non-linear optical properties [20] of some TTz derivatives have already been reported. However, the spectroscopic characterization of this compound only reports that the electronic absorption spectrum is centered at 356 nm and that the fluorescence emission in some solvents is centered at 410 nm [23].

The present work investigates the photophysical properties of DTTz in several solvents, including a strong acidic medium, and in the solid state using optical absorption and steady-state fluorescence spectroscopy. Quantum yield calculations are also reported. The results of optical spectroscopy are interpreted using quantum mechanical calculations performed with Gaussian'98 [28] that successfully explains the fluorescence spectrum in acidic solution. Moreover, the experimental Stokes's shift of the absorption (excitation) and fluorescence bands is interpreted in terms of the Lippert's equation [29] for DTTz in solution and on the bases of the exciton theory for the solid state system [30].

2. Experimental

2.1. Materials

Dithiooxamide (Aldrich Chemical Co.) was employed for the synthesis of DTTz and was used as received. The spectroscopic grade solvents acetonitrile, cyclohexane, chloroform, dimethylformamide, diethyl ether, ethanol, isopentane, and trifluoracetic acid were initially dried with 3 Å molecular sieves. Acetonitrile, cyclohexane, chloroform, diethyl ether and isopentane were treated with phosphorous pentoxide and then distilled over a small amount of basic aluminum oxide. Methanol was distilled over Mg/I_2. Dimethylformamide and dimethylsulfoxide (DMSO) was distilled over a small amount of polymeric methylene-bis-phenylene isocyanate (MDI) under vacuum. Trifluoracetic acid and benzaldehyde were distilled prior to use. All the solvents were sonicated under vacuum, saturated with argon and storaged in the dark before use. 9,10-Diphenylanthracene (DPA) (Aldrich Chemical Co.) was vacuum sublimated, and then crystallized from ethanol. DTTz was synthesized according to a procedure described elsewhere [17,18,23]. Other chemicals were used without further purification.

Solutions of DTTz and DPA were prepared in several solvents just prior to the emission measurements in the concentration range of ca. 10^{-5} to 10^{-3} mol l^{-1}. They were degassed by sonication under vacuum and saturated with argon. All solutions were degassed by several freeze-thaw cycles and stored under argon in the dark before the fluorescence analysis.

2.2. Methods and characterization

Structural characterization of DTTz was performed by spectroscopic techniques. The infrared spectrum of DTTz in a KBr pellet was recorded using a Bomem B100 FTIR spectrophotometer. The spectrum resolution was 2 cm^{-1} over the spectral range 400–4000 cm^{-1}, using an accumulation of 16 scans. ^1H and decoupled ^{13}C-NMR spectra of a $CDCl_3$ solution was performed using a Bruker AC300/P operating at 300 and 75.45 MHz, respectively.

DTTz was purified by preparative chromatography using a Spherisorb cyano-silica column (Sigma) with linear gradient elution from 100% cyclohexane to 100% 1,4-dioxane in 25 min. HPLC runs were done on a WATERS 600E chromatograph with U6K injector, WATERS 410 differential refraction index and WATERS 991 UV–VIS detectors. The sample is >99.9% pure by subsequent HPLC analysis.

This procedure yielded a sample with melting point of 215.8°C, measured using a differential scanning calorimeter (DSC) (Perkin Elmer DSC-7 series) calibrated with indium. The scan was performed with a heating rate of 20°C min^{-1}. The thermal stability of DTTz was determined by thermogravimetric analysis using a Perkin Elmer TGA-7 analyzer, scanned from 30 to 700°C at heating rate of 20°C min^{-1} under N_2.

Electronic absorption UV–VIS spectra were recorded at room temperature using a HP8542A spectrophotometer with a photodiode array detector. A 1 cm square quartz cuvette was used for measurements of solutions.

Excitation and fluorescence spectra at room temperature and at 77 K were recorded in a PTI LS100 (Photon

Technology) spectrofluorimeter operating in the steady-state mode, with resolution of 2.0 nm. The corrected spectrum was obtained using an experimental correction factor determined by comparison of the experimental DPA and the true DPA fluorescence spectra, in the spectral range from 360 to 550 nm [31]. A 1 cm square quartz cuvette equipped with an argon venting system at the top was used for measurements of the spectrum of the solutions. The spectrum of samples in the solid state was recorded using a thin layer of DTTz crystals prepared by vapor deposition on the frontal face of the cuvette. Low temperature (77 K) spectra were obtained from an EPA (ethanol–isopentane–ether mixture) glass solution using a 5.0 mm diameter quartz tube placed in a Dewar flask with a quartz window. The spectrum was recorded after several freeze-thaw cycles under vacuum to degas the samples.

2.3. Computational methods

The geometry of DTTz was optimized by the Hartree–Fock (HF) method using the 6-31G basis set (HF/6-31G). The rotational barrier of the phenyl ring in DTTz (Scheme 1) was calculated by the density functional method, B3LYP with 6-31G* basis set. The B3 functional is the Becke's three parameter functional method [32] and LYP is Lee, Yang and Parr's correlation functional method [33]. The basis set is 31 split-valence with polarization functions. Excitation energies and oscillator strengths of the electronic transitions of DTTz were calculated using the semi-empirical ZINDO [34] method. No solvent effects were included in the calculations. Simulation of the spectra was made with the software SPECTRUM.C [35] using Gaussian lineshape, a half-width at half-maximum (HWHM) value of 12.5 nm and a frequency step size of 1 nm.

3. Results and discussion

As previously described, DTTz may be synthesized by a one-step condensation reaction between benzaldehyde and dithiooxamide using two different experimental protocols: one that mixes both components and heats the system at high temperature, and the other that refluxes the precursors in *N*,*N*-dimethylformamide. The latter gives a higher yield and furnishes better product purity and, thus, was employed in the present work. Since spectroscopic purity grade is required in the present work, we performed the synthesis under milder conditions and shorter reaction times (10–15 min) in order to avoid secondary reaction products. Moreover, we employed further purification steps where the crude material was crystallized. Subsequently, the DTTz sample was sublimed under vacuum, dissolved in spectroscopic grade solvent, chromatographed using a cyano-silica column and then recrystallized three more times.

3.1. Thermal and photochemical stability

DSC scans showed one endothermic peak at 215.8°C (112.4 J mol^{-1}), which agrees with the melting point of reference [23]. No other mesomorphic transition was detected. Further, thermogravimetric analysis showed a sharp weight loss at 296.7°C, attributed to the vaporization of the whole sample. This explanation for the loss of weight was confirmed by heating the sample in a sealed glass tube under nitrogen at 320°C for 15 min in an oven. No apparent degradation was detected by analysis using FTIR and UV absorption spectroscopies, demonstrating that DTTz is a highly thermally stable compound.

A preliminary study by UV–VIS absorption spectroscopy evaluated the photostability of the DTTz in a dilute solution of methanol. The solution of DTTz was irradiated with an UV–VIS Hg high-pressure arc lamp for 10 h. After 1 h of irradiation, a spectrum was collected. They showed virtually the same absorption spectrum profile demonstrating that DTTz is also a photostable compound in solution under this experimental condition.

3.2. Absorption spectra

Fig. 1a shows the electronic absorption spectra of DTTz in cyclohexane at 10^{-5} mol l^{-1}. The maximum of the band is centered at ca. 357 nm and the band exhibits a vibrational structure with at least two overlapped bands at 344 and 373 nm for all solvents (Table 1). A slight solvatochromic shift of the absorption maximum as a function of the solvent polarity is observed (Fig. 2). But no effective band broadening occurs. One possible explanation for the low vibrational resolution of the DTTz absorption spectrum is the occurrence of rotamerism around the C–C bond involving the phenyl and the thiazol rings. This rotation barrier of the phenyl ring was theoretically estimated as ca. 5.1 kcal mol (HF/6-31G//HF/6-31G) and ca. 5.5 kcal/mol (B3LYP/6-31G*//B3LYP/6-31G*). Both HF and DFT gave approximately the same value to the rotation barrier. Both seem very high to explain the broadening of the absorption bands by the presence of rotational conformers. Since no solvent effect was taken into account in these calculations, we should consider that the presence of solvent affects (and lowers) the height of the activation barrier. Thus, although the coplanar form of the molecule DTTz (Scheme 1) is the most stable, according to the quantum chemical calculation, several conformers may coexists in equilibrium at room temperature and, then, several ro-vibronic states of the ground state molecule, with similar energies, may be populated leading to a broadening of the band shape.

Fig. 1b shows a theoretical absorption spectrum simulated by quantum mechanics calculation. It is comparable with the observed spectrum shown in Fig. 1a. The simulated band reproduces the overall characteristics of the observed band fairly well. There is a strong band between 300 and

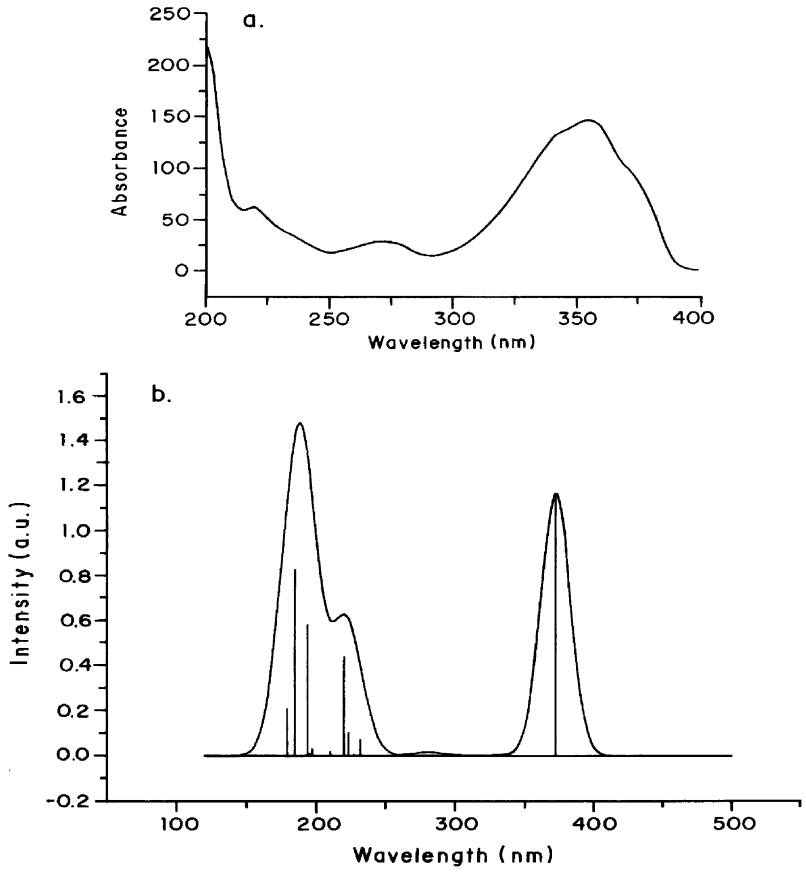

Fig. 1. (a) Electronic absorption spectra of DTTz in cyclohexane at 10^{-5} mol l^{-1}; (b) simulated spectrum calculated by quantum mechanics. A–D are described in the text.

400 nm (band A) in both observed and simulated spectra. It corresponds to a transition mainly due to π^*(LUMO) ← π(HOMO). HOMO consists of a π-orbital that spreads over the entire molecule with slight emphasis in the central, TTz moiety. LUMO is π^* orbital that concentrates mainly in the central TTz moiety. According to the calculation, the transition moment is polarized in the molecular plane (*xy*-plane) forming an angle of 17.1° from the *y*-axis, which is the short molecular axis (Scheme 1). The calculated transition energy corresponds to the strong band is 372.2 nm, which is compared to the observed value of 357 nm. The discrepancy between theory and experiment is due, partly, to the approximate nature of the theory and partly to the solvent effect, which the theory did not take it account. There is a low intensity band (band B) at ca. 270 nm in the experimental absorption spectrum (Fig. 1a) that also appears in the simulated spectrum: a low intensity band at the same region of ca. 280 nm. In addition, the UV-spectrum shows two other bands: band C as a shoulder of a very intense band D (Fig. 1a). Both the C and D bands are composite of several $\pi^* \leftarrow \pi$ transitions as seen in the simulated spectrum (Fig. 1b). The calculated peak positions for the C and

Table 1
Solvent dielectric constant, ε, and refractive index, n, absorbance and fluorescence maxima (nm), Stokes's shifts $\nu_A - \nu_F$ (cm^{-1}) and fluorescence quantum yields ϕ_F for DTTz

Solvent	ε	n	Absorbance λ_{max} (nm)[a]	Fluorescence λ_{max} (nm)[a,b]	Δf	$\nu_A - \nu_F$ (cm^{-1})	ϕ_F^d
Cyclohexane	2.02	1.4266	357.0	410.7	0.00	3662.53	0.25
Chloroform	10.0	1.4476	357.2	412.0	0.15	3739.36	0.16
Acetonitrile	29.7	1.3442	354.6	410.6	0.30	3846.19	0.23
Methanol	33.0	1.3288	353.6	411.5	0.31	3979.21	0.22
DMSO	47.2	1.4170	360.1	417.6	0.28	3823.70	0.16
Trifluoracetic acid	8.42		362.0	466.0	–	6165.08	–

[a] 10^{-5} mol l^{-1}.
[b] Excitation at 350 nm, Δf is defined by Eq. (3).

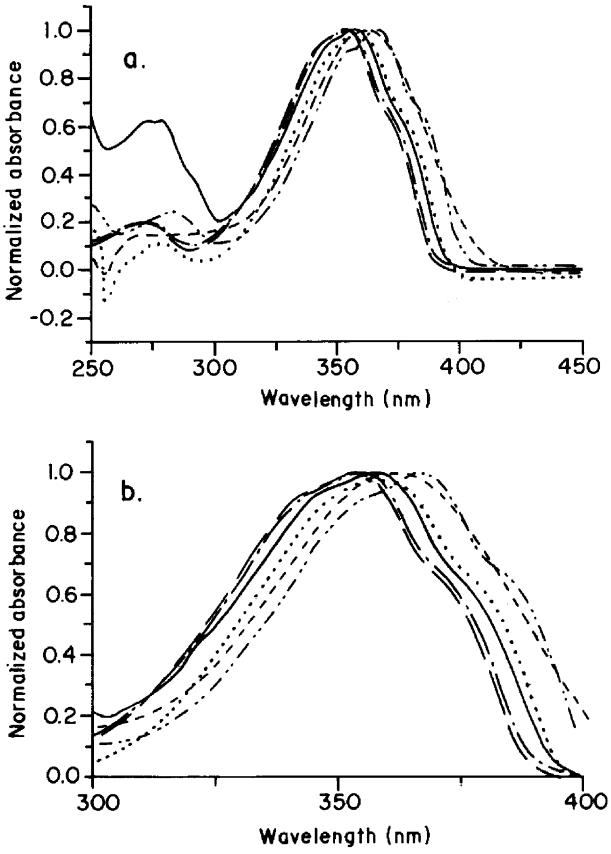

Fig. 2. (a) Electronic absorption spectra of DTTz in several solvents: cyclohexane (·····), chloroform (—), acetonitrile (— —), DMSO (·····), methanol (· · ·) and trifluoroacetic acid (- - -); (b) detail of the maximum of the bands. DTTz concentration: 10^{-5} mol l^{-1}.

D bands are located at ca. 220 and 184 nm, respectively, in agreement with the experimental data.

The solvatochromism effect may be visualized in Fig. 2 that shows the absorption band at 300–400 nm for DTTz dissolved in several solvents (cyclohexane, chloroform, acetonitrile, DMSO, methanol and trifluoroacetic acid). These spectra show that highly polar solvents, such as DMSO, stabilize the electronic ground state, producing a blue-shift of the band peak, while protic solvents, such as methanol, plays the opposite effect (red-shift).

The electronic absorption spectrum of DTTz in trifluoracetic acid solution exhibits a different form compared with other solvents (Fig. 2). The normalized absorbance spectrum in trifluoracetic acid presents a bathochromic effect ($\Delta\nu \approx 387\,\mathrm{cm}^{-1}$) and a broadening of the band with depletion of the structured vibronic absorption. To analyze this spectral behavior, we recorded the absorption spectra of DTTz in aqueous acid solutions of HCl with several concentrations (1–8 mol l^{-1}) (Fig. 3). A very similar spectrum is observed for both the trifluoroacetic acid solution and for the higher concentrations of HCl solutions (8–12 mol l^{-1}). Therefore, this absorption band is attributed to the ability of the trifluoracetic acid to protonate the nitrogen atom of the

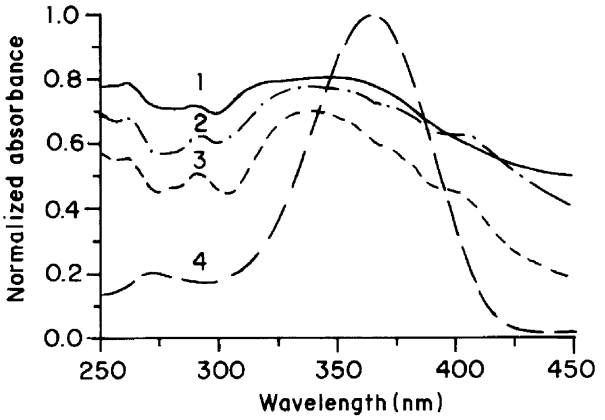

Fig. 3. Electronic absorption spectra of DTTz in aqueous HCl solutions: 1 mol l^{-1} (1); 4 mol l^{-1} (2); 6 mol l^{-1} (3); 8 mol l^{-1} (4). DTTz concentration: 10^{-5} mol l^{-1}.

thiazole groups, causing a higher stabilization of the HOMO, rather than the LUMO, and a red-shift of the absorption maximum.

Table 2 lists some of calculated lower lying singlet excited states, S_1–S_8, for both neutral DTTz and diprotonated DTTz, henceforth, designated as DTTz(2H$^+$). The calculation shows that the lower energy electronic transition $S_0 \rightarrow S_1$ is allowed for both the molecules DTTz and DTTz(2H$^+$) and the calculated transition energy for DTTz is 372.23 nm while the corresponding value for DTTz(2H$^+$) is 398.38 nm. Thus, upon protonation, the $S_0 \rightarrow S_1$ transition of DTTz shifts towards a longer wavelength. Moreover, this shift toward longer wavelength is calculated for DTTz, demonstrating that a double protonation is responsible for the experimental results.

Table 2
Some lower lying singlet excitation energies (E), wavelength (nm) and oscillator strength (f) of both DTTz and diprotonated DTTz(2H$^+$) calculated with ZINDO

Excited state	E (eV)	λ (nm)	f
DTTz			
S_1	3.3308	372.23	1.1722
S_2	4.1405	299.44	0.0000
S_3	4.1613	297.95	0.0000
S_4	4.3990	281.85	0.0108
S_5	4.4219	280.38	0.0004
S_6	4.4223	280.36	0.0000
S_7	5.1251	241.91	0.0000
S_8	5.3472	231.84	0.0737
DTTz(2H$^+$)			
S_1	3.1122	398.38	1.2300
S_2	3.5698	347.31	0.0054
S_3	3.5738	346.92	0.0854
S_4	3.6537	339.34	0.0001
S_5	4.6031	369.35	0.0000
S_6	4.8141	257.54	0.2438
S_7	4.8544	255.40	0.0006
S_8	5.3133	233.35	0.0008

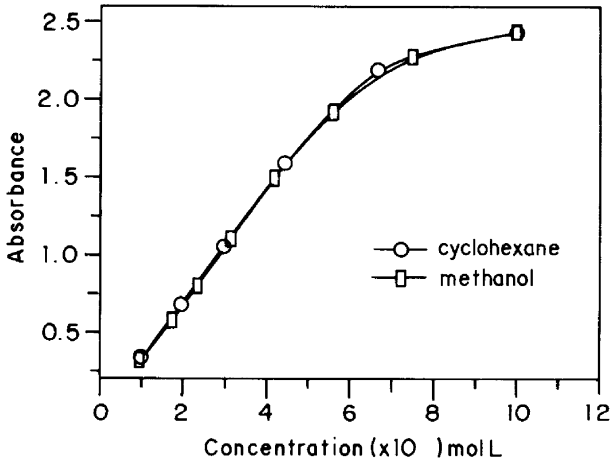

Fig. 4. Lambert–Beer's plot for the maximum absorbance of DTTz in cyclohexane

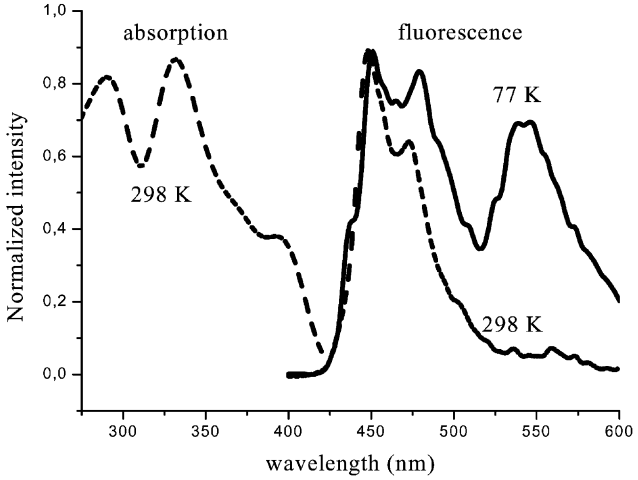

Fig. 6. Electronic absorption at 298 K and fluorescence emission at 298 and 77 K for DTTz in the solid state. $\lambda_{exc} = 360$ nm.

The absorption spectra are also recorded for DTTz in cyclohexane and methanol solutions, at several concentrations (10^{-5} to 10^{-4} mol l^{-1}) (Fig. 4). Typical Lambert–Beer plots are obtained and the deviation from linearity is observed at concentrations higher ca. 6×10^{-5} mol l^{-1}. The average molar absorptivity coefficient calculated for DTTz in several media is ca. $\varepsilon_{max} = 37,200\,l\,mol^{-1}\,cm^{-1}$. This value is almost insensitive to the solvent polarity, within the standard deviation.

In order to improve the vibrational resolution we recorded the absorption spectrum at low temperature (77 K) in a frozen glass of EPA (Fig. 5) [31]. This shows sharper vibrational bands, with strong vibrational progression at 885 cm^{-1}. This vibrational mode is also present in the FTIR spectrum (880 cm^{-1}), corresponding to the heterocycle-stretching mode. A similar progression is reported for model compounds such as TTz (860 cm^{-1}) [36]. The coincidence with the value determined by FTIR (888 cm^{-1}) is a strong indication that there is no molecular geometry distortion upon electronic excitation.

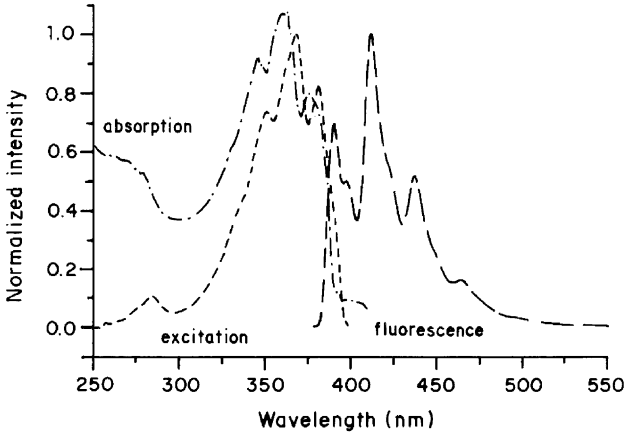

Fig. 5. Electronic absorption (-·-·-), excitation (- - -) and fluorescence (– –) spectra of DTTz in EPA glass, at 77 K. DTTz concentration: 10^{-5} mol l^{-1}. $\lambda_{em} = 410$ nm, $\lambda_{exc} = 350$ nm.

The solid state absorption spectrum is broader and the blue-shift is comparable with that in glass EPA (Fig. 6). When both are compared, at the same temperature, we observe a exciton splitting of the lower energy absorption band into two: one with lower intensity and lower energy ($\lambda_{II} = 394$ nm) and the other with a higher energy ($\lambda_{I} = 332$ nm) and higher intensity. We interpret this result on the basis of the exciton theory for dimeric specimen formation where the relative orientations of the two molecules in the solid state present a parallel orientation of the dipole moments in a π-stagger configuration [30]. Considering this excitonic model and this architecture for the molecules in the solid state, the expected transition rule establishes that the lower energy transition is forbidden (lower intensity) while the higher energy transition is allowed (higher intensity). The exciton splitting of the excited states leads to the appearance of an exciton singlet state that lies below to that of the monomeric dye molecule. According to the Kasha's rule, the fluorescence emission should be shifted to the red either at room or lower temperatures [30], although it is a forbidden transition for this type of aggregates. In addition to this exciton emission (420–500 nm), we also observed an emission centered at 550 nm, whose intensity is enhanced at low temperature (77 K). Although we have not recorded the time resolved spectra, we think that this emission should be attributed to the phosphorescence in the solid state. The reason for this assumption is the well-known enhancement of the intersystem crossing in systems probability due to exciton splitting [30].

3.3. Photoluminescence properties

Fluorescence and excitation spectra of DTTz in several solvents and at low concentration (10^{-5} mol l^{-1}) were

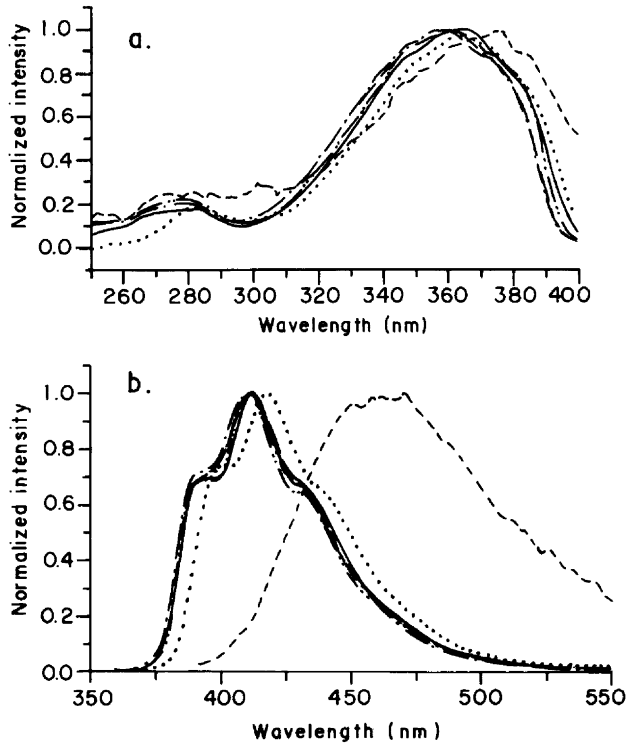

Fig. 7. (a) Excitation (λ_{em} = 410 nm) and (b) fluorescence (λ_{exc} = 350 nm) spectra of DTTz in several solvents: cyclohexane (·····), chloroform (—), acetonitrile (— —), DMSO (·····), methanol (· · ·) and trifluoroacetic acid (- - -); (b) detail of the maximum of the bands. DTTz concentration: 10^{-5} mol l^{-1}.

recorded using $\lambda_{exc} = 350$ and $\lambda_{em} = 410$ nm, respectively (Fig. 7). As noticed, the excitation spectrum of DTTz in a specific solvent presents a similar profile to the absorption spectra and also exhibits a similar solvatochromism with the solvent properties. Thus, it exhibits a small red-shift with increase of the polarity of the solvent. The transition is assigned to $\pi^* \rightarrow \pi$ ($S_1 \rightarrow S_0$), based on the small solvatochromic shift observed for the fluorescence spectra. The emission spectra centered at 410 nm exhibit two additional vibrational bands at 394 and 430 nm, except for trifluoracetic acid. Moreover, the fluorescence spectra in all solvents are mirror images of the excitation (absorption) spectrum, indicating that a similar geometry is involved in both electronic ground and excited states [31]. The relative intensities of the vibrational bands are almost independent of the polarity of the solvent. This implies that no significant geometrical distortion of the molecule is present, in agreement with the reported data for the fluorescence spectra of benzothiazole and bithiazole derivatives [16].

The fluorescence quantum yield of DTTz in several solvents at a concentration of 10^{-5} mol l^{-1} was determined and the values are collected in Table 1. This determination is based on the comparison with a 10^{-6} mol l^{-1} solution of DPA in cyclohexane as a quantum yield standard, using the equation [31]:

$$\phi_F \text{ (chromophor)} = \phi_{DPA} \frac{A_{DPA}}{A_{chrom}} \frac{F_{chrom}}{F_{DPA}} \left(\frac{n_{solv}}{n_{cycloh}} \right)^2 \quad (1)$$

where $\phi_{DPA} = 1$ is the fluorescence quantum yield of DPA in cyclohexane [31], A_{DPA} and A_{chrom} are the molar absorptivity of DPA and DTTz at 350 nm, respectively and F_{DPA} and F_{chrom} are the integrated area of corrected fluorescence emission for the DPA and DTTz, respectively.

An average value of $\phi = 0.23 \pm 0.02$ was obtained for DTTz in cyclohexane, acetonitrile and methanol solutions. The lowest value of $\phi = 0.16 \pm 0.02$ was observed for DMSO and chloroform solutions. Errors of ±15% are expected in this determination. There are several possible explanations for the lower values obtained for DTTz in these two solvents: (1) occurrence of some photochemical reaction; (2) occurrence of quenching of the fluorescence by residual molecular oxygen that might be still present although there were several attempts to remove it; (3) lower solubility in these solvents, leading to a self-quenching process; (4) the external heavy atom effect produced by the heteroatom of the solvent molecule. At the present we are not able to distinguish among these possibilities, although we believe that the possibilities of photochemical reactions or quenching by molecular O_2 are less probable.

The solvatochromic shift due to the polarity effects of the solvent is analyzed on the basis of the Lippert's equation that correlates the Stokes's shifts with the solvent properties [29,31]:

$$\nu_A - \nu_F = \frac{2}{hc} \left(\frac{\varepsilon - 1}{2\varepsilon + 1} - \frac{n^2 - 1}{2n^2 + 1} \right) \frac{(\mu_E - \mu_G)^2}{a^3} \quad (2)$$

where ν_A and ν_F are the wave numbers (cm^{-1}) of the maximum absorption and emission, respectively observed for a given solution, ε and n are the dielectric constant and the refractive index of the solvent, respectively, a is the radius of the cavity surrounded by solvent molecules and μ_E and μ_G are the dipole moments for the excited and ground states, respectively.

The term (Δf) is defined as the polarizability of the solvent, which gathers the electronic response of the solvent, expressed by the refractive index and the orientation of the solvent dipole in the excited state, expressed by the dielectric constant value (Eq. (3)) [29]:

$$\Delta f = \frac{\varepsilon - 1}{2\varepsilon + 1} - \frac{n^2 - 1}{2n^2 + 1} \quad (3)$$

The orientation polarizability (Δf) and the respective Stokes's shifts observed for diluted solutions of DTTz are listed in Table 1. A good linear correlation between ($\nu_A - \nu_F$) versus Δf (Fig. 8) is obtained, with the exception of DTTz in methanol, a protic solvent, confirming that specific interaction such as hydrogen bonding between solvent and the dye cannot be well represented by the Lippert's equation

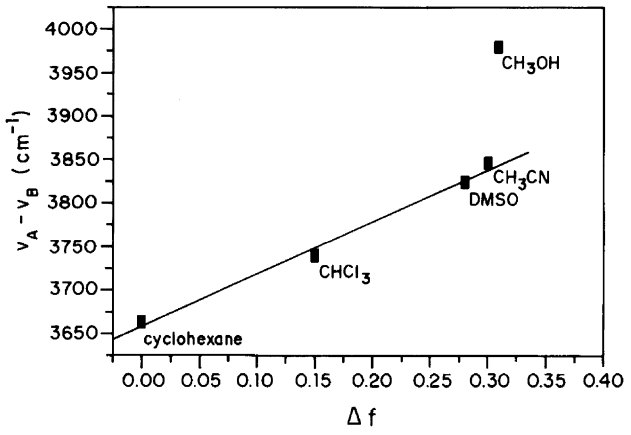

Fig. 8. Lippert's plot for the Stokes's shift ($\nu_A - \nu_F$) of DTTz in several solvents. The Δf is defined in terms of the Lippert's Eq. (3).

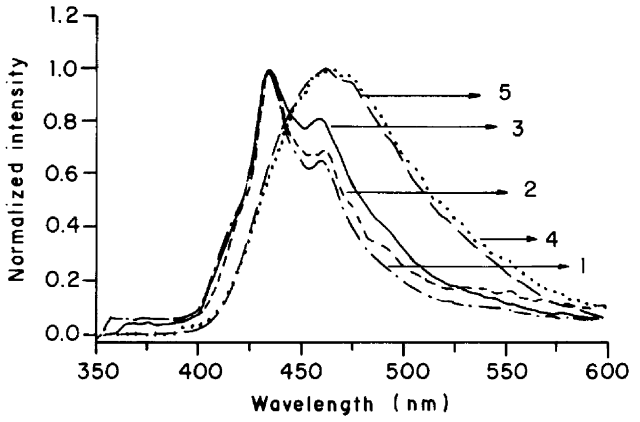

Fig. 9. Fluorescence spectra of DTTz in aqueous HCl solutions: 1 mol l^{-1} (1); 4 mol l^{-1} (2); 6 mol l^{-1} (3); 8 mol l^{-1} (4); 12 mol l^{-1} (5). DTTz concentration: 10^{-5} mol l^{-1}.

[29]. For this reason, the Stokes's shift of DTTz in trifluoracetic acid solution was not analyzed because the protonated species behaves abnormally.

The slope of the Lippert's plot (Fig. 8) gives the value, $\Delta\mu_{E\rightarrow G}$, for the difference between the dipole moment of excited and ground states of the molecule, if the value for the radius of the cavity, *a*, is known. Precise determination of *a* is a difficult task. This value is usually estimated using molecular volume calculation [37,38]. Following this approach, we calculated its molecular volume as 244.4 $Å^3$ using the SURF program [39]. If we assume that the molecule is spherical, we are able to calculate its radius as an approximation to the radius of the cavity, *a*. The estimated *a* value is 3.88 Å. Using this approximate value and the slope values of the Lippert's plot, we calculate the difference between the ground and excited states dipole moments, $\Delta\mu_{E\rightarrow G}$, as 2.64 D. The theoretical value of the dipole moment, obtained using both the DFT B3LYP/6-31G*//B3LYP/6-31G* and HF/6-31G//HF/6-31G, of DTTz in its ground state was 0 D. The dipole moment of the molecule in its ground state is expect to be null due to its high molecular symmetry. Thus, the dipole moment of the excited state of the molecule is approximately 2.64 D, showing that upon electronic excitation a substantial increase of the dipole moment is occurring. Consequently, the excited state should be more stabilized in a polar solvent than in a non-polar solvent. This explains the red-shift of the fluorescence band for DTTz in more polar solvents, such as DMSO.

The fluorescence emission of DTTz in a solution of trifluoracetic acid exhibits a remarkable spectral red-shift (Fig. 9) with a dramatic decrease of the emission intensity in comparison to the other solvents, including methanol (Fig. 7). The fluorescence quantum yield for this emission was estimated to be less than 0.05 (Table 1) using the same approach as previously described. The changes of the spectral profile are attributed to the diprotonation of the nitrogen atom of the heterocyclic ring of the DTTz, as also evidenced by the electronic absorption spectrum. The dipole moment for the DTTz($2H^+$) in the electronic ground state, calculated using HF/6-31G//HF/6-31G, is 0.14 D. Thus, the increase of dipole moment going from neutral DTTz to DTTz($2H^+$) is only ca. 0.14 D. Despite the similarity between the dipole moments for DTTz and its diprotonated form, there is a large red-shift of the fluorescence band in such a polar environment. This result is explained by the increase of the dipole moment upon excitation that is associated with an effective intramolecular charge transfer in the excited state.

According to Kasha's rule, the fluorescence emission should take place from the S_1 state [31]. The separation between S_1 and S_2 of the neutral DTTz is 0.810 eV and the S_3 state is almost degenerate to S_2. Oscillator strength of the transitions to S_1–S_3 of DTTz($2H^+$) are 0.790, 0.005, and 0.085, respectively and the energy gap between S_1 and S_2 is lower, 0.458 eV (Table 2). Moreover, the energy gap between S_1 and S_3 is only 0.462 eV. Upon the protonation, the separation between S_1 and S_2 decreases almost to half of that corresponding to neutral DTTz. The oscillator strength of S_2 (and S_3) also increases from 0 in DTTz to 0.005 (and 0.085) upon protonation. Similar effects might be produced in the triplet electronic states. Thus, the observed lower intensity emission of DTTz($2H^+$) may be due to the proximity effect, the decrease of the separation between S_1 and S_2(or S_3), and the increase of oscillator strengths of S_2(or S_3), in comparison to neutral DTTz. This can be due to the increase of the energy levels of the protonated non-bonding orbital located on the nitrogen atom and the π^* orbital involved in the π–π^* transition [31,40].

In order to get further insights into the mechanism of the fluorescence emission of DTTz in acid media, we measured the fluorescence spectra of this molecule in an aqueous solution of hydrochloric acid at different concentrations (Fig. 9). A similar lower energy and structureless band centered at 460 nm are observed for aqueous strongly acidic media (8 and 12 mol l^{-1} HCl solutions), as also observed for trifluoroacetic acid. For less acidic media the fluorescence spectra are similar to those observed for DTTz in solid state (Fig. 6).

Thus, there is a strong indication that DTTz exhibits a significant solubility only in strongly acidic aqueous media, although it is almost completely aggregated in weakly aqueous acidic ones.

4. Conclusions

The photophysical properties of DTTz in several solvents were determined by steady-state fluorescence spectroscopy. The Stokes's shift of the electronic absorption and fluorescence spectra are well described by the Lippert's equation for non-protic solvents. The similarities between the experimental and simulated absorption spectra demonstrate that the quantum mechanic methodology successfully describes the energy levels for this molecule. The calculation was also very useful to interpret the electronic spectra of this dye in strongly acidic medium. A diprotonated molecule is present under these conditions. This calculation demonstrates that there are changes of the energy gaps involved with the electronic transitions and the decrease of the fluorescence quantum yield may be explained by the proximity effect. The low solubility in acid solutions produces a fluorescence spectrum characteristic of the solid state. The π-stagger orientation of the molecules explains the exciton splitting observed for the solid state fluorescence.

The quantum mechanical calculation, the small Stokes's shift in several solvents, the high planarity of the two fused thiazole rings, the vibrational structure leading to a mirror image of the excitation (absorption) and fluorescence spectra support the conclusion that electronic π–π^* transition are involved with the UV–VIS spectra of this molecule.

Acknowledgements

T.D.Z. Atvars and Y. Takahata thank FAPESP for the research grants and CNPq for the fellowships. M. R. Pinto gratefully acknowledges a fellowship from FAPESP. The authors thank Prof. Carol Collins for useful discussions.

References

[1] S.L. Murov, I. Carmichel, G.L. Hug, Handbook of Photochemistry, Marcel Dekker, New York, 1993.
[2] F. Cacialli, X.C. Li, R.H. Friend, S.C. Moratti, A.B. Holmes, Synth. Met. 75 (1995) 161.
[3] J.P. Ferraris, D.J. Guerrero, Recent advances in heteroaromatic copolymers, in: T.A. Skotheim, R.L. Elsenbaumer, J.R. Reynolds (Eds.), Handbook of Conducting Polymers, Marcel Dekker, New York, 1998.
[4] M. Meier, E. Buchwald, S. Karg, P. Posch, M. Greczmiel, P. Strohriegl, W. Rieß, Synth. Met. 76 (1996) 95.
[5] Y. Yang, Q. Pei, J. Appl. Phys. 77 (1995) 4807.
[6] M. Strukelj, F. Papadimitrakopoulos, T.M. Miller, L.J. Rothberg, Science 267 (1995) 1969.
[7] J.I. Nanos, J.W. Kampf, M.D. Curtis, Chem. Mater. 7 (1995) 2232.
[8] T. Yamamoto, H. Suganuma, T. Marayama, K. Kutoba, J. Chem. Soc., Chem. Comm. 16 (1995) 1613.
[9] Y.H. Jeffrey, K. Politis, H. Cheng, M.D. Curtis, J. Kanicki, IEEE Trans. Electron Devices 44 (1997) 1282.
[10] T. Yamamoto, H. Suganuma, T. Maruyama, T. Inoue, Y. Muramatsu, M. Arai, D. Komarudin, N. Ooba, S. Tomaru, S. Sasaki, K. Kubota, Chem. Mater. 9 (1997) 1217.
[11] I. Petkov, T. Deligeorgiev, I. Timtcheva, Dyes and Pigments 35 (1997) 171.
[12] T. Yamamoto, N. Hayashida, Reactive Functional Polym. 37 (1998) 1.
[13] A. Rossler, P. Boldt, J. Chem. Soc., Perkin Trans. 1 (1998) 685.
[14] P.N. Prasad, B.A. Reinhardt, Chem. Mater. 2 (1990) 660.
[15] J.F. Wolfe, B.H. Loo, F.E. Arnold, Macromolecules 14 (1981) 915.
[16] Y.H. So, J.M. Zaleski, C. Murlick, A. Ellaboundy, Macromolecules 29 (1996) 2783.
[17] J.R. Johnson, R. Ketcham, J. Am. Chem. Soc. 82 (1960) 2719.
[18] J.R. Johnson, D.H. Rotenberg, R. Ketcham, J. Am. Chem. Soc. 93 (1970) 4046.
[19] R. Bossio, S. Marcaccini, P. Pepino, T. Torroba, G. Valle, Synthesis 12 (1987) 1138.
[20] A. Rossler, P. Boldt, J. Chem. Soc., Perkin Trans. 1 (1998) 685.
[21] A. Bolognesi, M. Catellani, S. Destri, W. Porzio, Acta Cryst. C43 (1987) 2108.
[22] F.S. Biseca, Rev. Latinoamer. Quím. 21 (1990) 102.
[23] D.A. Thomas, J. Heterocycl. Chem. 7 (1970) 457.
[24] L. Nygaard, E. Asmussen, J.H. Høg, R.C. Maheshwari, C.H. Nielsen, I.B. Petersen, J.R. Andersen, G.O. Sørensen, J. Mol. Struct. 8 (1971) 225.
[25] J. Bartulin, C. Zuniga, H. Muller, T.R. Taylor, Mol. Cryst. Liquid Cryst. 180 (1990) 297.
[26] Y.Z. Yousif, A.J.A. Hamdani, Liquid Cryst. 15 (1993) 451.
[27] M. Catellani, S. Destri, W. Porzio, B. Thémans, J.L. Brédas, Synth. Met. 26 (1988) 259.
[28] M.J. Frish, G.W. Trucks, H.B. Schlegel, G.E. Scuseria, M.A. Robb, J.R. Cheeseman, V.G. Zakrzewski, J.A. Montgomery, R.E. Stratmann, J.C. Burant, S. Dapprich, J.M. Milliam, A.D. Daniels, K.N. Kudin, M.C. Strain, O. Farkas, J. Tomasi, V. Barone, M. Cossi, R. Cammi, B. Mennucci, C. Pomelli, C. Adano, S. Clifford, J. Ochterski, G.A. Peterson, P.Y. Ayala, Q. Cui, K. Morokuma, D.K. Malick, A.D. Rabuck, K. Ragavachari, J.B. Foresman, J. Cisolwski, J.V. Ortiz, B.B. Stefanov, G. Liu, A. Liashenko, P. Piskorz, I. Komaromi, R. Gompertz, R.L. Martin, D.J. Fox, T. Keith, A. Al-Laham, C.Y. Peng, N. Nanayakkara, C. Gonzalez, M. Challacombe, P.M.W. Gill, B.G. Jonson, W. Chen, M.W. Wong, J.L. Andres, M. Head-Gordon, E.S. Replogle, J.A. Pople, Gaussian'98, Revision A.1, Gaussian Inc., Pittsburgh, PA, 1998.
[29] C. Reichardt, Solvent and Solvent Effects in Organic Chemistry, 2nd Edition, VCH, Weinheim, 1988.
[30] M. Kasha, H.R. Rawls, M.A. El-Bayomi, Pure Appl. Chem. 75 (1965) 371.
[31] J.R. Lackowicz, Principles of Fluorescence Spectroscopy, Plenum, New York, 1999.
[32] A.D. Becke, J. Chem. Phys. 98 (1993) 5648.
[33] C. Lee, W. Yang, R.G. Parr, Phys. Rev. B37 (1988) 785.
[34] M.C. Zerner, Semi-empirical molecular orbital methods, in: K.B. Lipkowitz, D.B. Boyd (Eds.), Reviews of Computational Chemistry, Vol. 2, VCH, New York, 1991, p. 313.
[35] P.D. Soper, DuPont, Central Research and Development, E328/123, DUCOM 695-1757, ESVAX, SOPERPD.
[36] A. Brillante, B. Samori, C. Stremmenos, P. Xanirato, Mol. Cryst. Liquid Cryst. 100 (1983) 263.
[37] J.J. Aaron, M.D. Gaye, J. Mol. Struct. 156 (1987) 119.
[38] P. Suppan, Chem. Phys. Lett. 94 (1983) 272.
[39] A.C. Gaudio, Y. Takahata, Comput. Chem. 16 (1992) 277.
[40] C. A Caetano, M.-A. De Paoli, T.D.Z. Atvars, F.B.T. Pessine, An. Acad. Bras. Cienc. 58 (1986) 531.